Universidade Federal de Juiz de Fora
Faculdade de Engenharia - Departamento de Engenharia de Produção e Mecânica
Curso de Graduação em Engenharia Mecânica

Lucas Pereira Verneck da Silva

Type-1 Fuzzy Logic System Applied to Classification of Rail Head Defects

Juiz de Fora
2017

Lucas Pereira Verneck da Silva

Type-1 Fuzzy Logic System Applied to Classification of Rail Head Defects

Trabalho de Conclusão de Curso apresentado ao Curso de Graduação em Engenharia Mecânica da Universidade Federal de Juiz de Fora, na área de concentração de Engenharia Mecânica, como requisito parcial para a obtenção do título de Bacharel em Engenharia Mecânica.

Orientador: Eduardo Pestana de Aguiar

Coorientador: Renan Piazzaroli Finotti Amaral

Juiz de Fora

2017

Ficha catalográfica elaborada através do Modelo Latex do CDC da UFJF
com os dados fornecidos pelo(a) autor(a)

Pereira Verneck da Silva, Lucas.
Type-1 Fuzzy Logic System Applied to Classification of Rail Head Defects / Lucas Pereira Verneck da Silva. – 2017.
34 f. : il.

Orientador: Eduardo Pestana de Aguiar
Coorientador: Renan Piazzaroli Finotti Amaral
Trabalho de conclusão de curso – Universidade Federal de Juiz de Fora, Faculdade de Engenharia - Departamento de Engenharia de Produção e Mecânica. Curso de Graduação em Engenharia Mecânica, 2017.

1. Type-1. 2. Fuzzy Logic Systems. 3. Image Processing. 4. Adaptive Algorithms. 5. Rail Head. I. Pestana de Aguiar, Eduardo, orient. II. Piazzaroli Finotti Amaral, Renan , coorient. III. Título.

Lucas Pereira Verneck da Silva

Type-1 Fuzzy Logic System Applied to Classification of Rail Head Defects

Trabalho de Conclusão de Curso apresentado ao Curso de Graduação em Engenharia Mecânica da Universidade Federal de Juiz de Fora, na área de concentração de Engenharia Mecânica, como requisito parcial para a obtenção do título de Bacharel em Engenharia Mecânica.

Aprovado em 10 de Novembro de 2017.

BANCA EXAMINADORA

Prof. Dr. Eduardo Pestana de Aguiar - Orientador
Universidade Federal de Juiz de Fora

Prof. Me. Renan Piazzaroli Finotti Amaral - Coorientador
Universidade Federal de Juiz de Fora

Prof. Dr. Alexandre da Silva Scari
Universidade Federal de Juiz de Fora

Prof. Dr. Moisés Luiz Lagares Júnior
Universidade Federal de Juiz de Fora

ACKLOWLEDGMENT

First of all, I would like to thank God for enlightening my path and being present in all moments of my life.

To my parents and my brother, for the unconditional love, affection, dedication, support and for the formation of my character.

To the professor, advisor and friend Eduardo Pestana de Aguiar for the support, incentive and for giving me the opportunity to develop this research. I am grateful for all knowledge acquired and for all past teachings.

To my girlfriend, who was always by my side, being a partner for every moment supporting me to go on.

To my coworkers at the laboratory who helped me during this research journey and development of this work.

To all my friends who have somehow been a part of this walk during these six years. No doubt each of you has had a part of it.

And finally, thank you Federal University of Juiz de Fora for making this all possible.

Never walk on the traveled path because
it only leads where others have been.
Alexander Graham Bell.

ABSTRACT

This work focuses on the classification of rail head defects, through images acquired by a rail inspection vehicle. With this regards, we discuss the use of a type-1 and singleton/non-singleton fuzzy logic system to dealing with this problem, based on a numerical data set composed of images provided by a Brazilian railway company, which covers the four possible rail head defects (cracking, flaking, head check and spalling). We use geometric correction through a two-dimensional affine transformation and a gray level co-occurrence matrix to extract the features to be used as an input of the classifiers. Finally, we present performance analysis in terms of classification ratio and convergence speed. The reported results show that the chosen non-singleton model result in improved efficiency and it can be used to handle uncertainties associated with this kind of problem.

Key-words: Type-1. Fuzzy Logic Systems. Image Processing. Adaptive Algorithms. Rail Head.

LIST OF FIGURES

LIST OF TABLES

LIST OF ABBREVIATIONS

FBF	Fuzzy Basis Function
FLS	Fuzzy Logic System
GLCM	Gray Level Co-Occurrence Matrix
T1-FLS	Type-1 Fuzzy Logic System
T2-FLS	Type-2 Fuzzy Logic System

SUMMARY

1 INTRODUCTION

Railways are a network of distributed rails which aims to connecting cities, states and countries. In most cases, they have been used for heavy loads, what impacts directly on rails, increasing its defects through material fatigue. Researches have been made to solve relevant questions in railways. As consequence, there is a increasing interest in transportation researchers to exploiting the feasibility of applying image processing and computational intelligence paradigms to address critical problems in order to improve the efficiency, safety, and environmental compatibility of transportation systems. Some problems, as detection of surface defects on rails, have been widely approached.

An intelligent vision detection system for discrete surface defects and focuses on image enhancement and automatic thresholding was discussed in [1]. Moreover, [2] proposed an automatic method for detecting one specific type of railway surface defect called squatsusing axle box acceleration measurements on trains. The authors in [3] presented and validated a fuzzy diagnosis method based on image processing, basing in an evaluation and integration between images obtained from camera and depth data measured with laser meter. In [4] is discussed an inspection method for rail surface defects based on automated machine vision system, analyzing two kinds of defect images including spalling of rail head and cracks in surface. In addition, [5] addresses the heavy rail surface defect detection according to their characteristics, uneven brightness and noise, and uses mathematical morphology of multi-scale and dual-structure elements as detection bases. In [6], the authors presented a new vision based on inspection technique for detecting special rolling contact fatigue defects that particularly occur on rail head surface, implementing an automatic detection system.

This work focuses on classify types of rail head surface defects that are commonly studied due to its severity and occurrence: cracking [7], flaking [8], head-check and spalling [9]. Researches have tried to improve the classification of these defects, using several different techniques, such as geometrical approach [6], gabor filter with texture analysis [10], image segmentation [4], based on visual inspection [11] and many others.

The fuzzy logic system (FLS) has been widely applied in classification problems due of their treatment of uncertainty, thus generating interesting results in several areas of the railway industry, as mentioned in [12, 13]. Although T1-FLS offer improved performance, certain kind of uncertainties associated with the classification problem is something that, unfortunately, T1-FLS can not properly handle. Additionally, the author in [14] stated that T2-FLS are computationally intensive because the type-reducer is very intensive. As a result, its training phase is extremely computational intensive.

The drawback associated with former techniques is the high computational complexity for training [14]. Considering a limited number of epochs, the training with reduced

computational complexity, high accuracy and high convergence speed consists in a hard task. The hardness is associated with the limited hardware resources is worsen and real time constraint.

The main contributions of this work are summarized as follows:

- We approach four types of defects that can occur in a rail head surface. The combined study of cracking, flaking head-check and spalling linked to rail head surface has never been addressed before.
- We use geometric correction through a two-dimensional affine transformation to facilitate the image processing and a gray level co-occurrence matrix (GLCM) to analyse textures on images.
- We employ the Type-1 singleton and non-singleton FLS, both trained by Steepest Descent method, in order to make a comparative analysis between the techniques.
- We present performance analyzes in terms of classification ratio and convergence speed by using a data set constituted by images acquired from a rail inspection vehicle provided by a company in the region that operates in the railway sector.

Our major conclusions are as follows:

- The two-dimensional affine transformation geometric correction and feature extraction through GLCM is effective for the current application.
- The classification ratio yielded by the non-singleton model is higher than those obtained with the singleton when a higher degree of uncertainties is presented in the input data.

The proposed model makes it possible to reduce the impact on trains operation and on preventive maintenance, since the interventions are performed at specific sites where the defect was detected. The model responsible for classifying the type of defect shall assist to:

- eliminate visual inspection of the rails and images acquired by the equipment;
- reduce the number of unproductive hours in maintenance, due to the knowledge of defects before moving the maintenance team to the field;
- reduce the number of recurrent preventive interventions;
- increase productivity of rail operations, given the reduction in time of operational maintenance.

2 PROBLEM FORMULATION

Among all possible defects that can occur on the rail head, the four main ones are cracking, flaking, head check and spalling. Let $\mathbf{A} \in \mathbb{R}^{n \times m}$ be a matrix constituted by elements of an image of the rail head. Figure 1 shows the paradigm used for the classification of events. In the block "Geometric Correction", $\mathbf{P}$ refers to cracking, flaking, head check, spalling and normal condition of the rail head. The block "Feature Extraction" provides extracted features $\mathbf{K}_{p_c}$, $\mathbf{K}_{p_f}$, $\mathbf{K}_{p_h}$, $\mathbf{K}_{p_s}$ and $\mathbf{K}_{p_n}$ vectors from $\mathbf{P}$. The block "Classification" applies one of the classification techniques discussed in this work to obtain the output vector $\mathbf{S}$, thereby identifying the type of defect. We use five independent classifiers, one for each possible event.

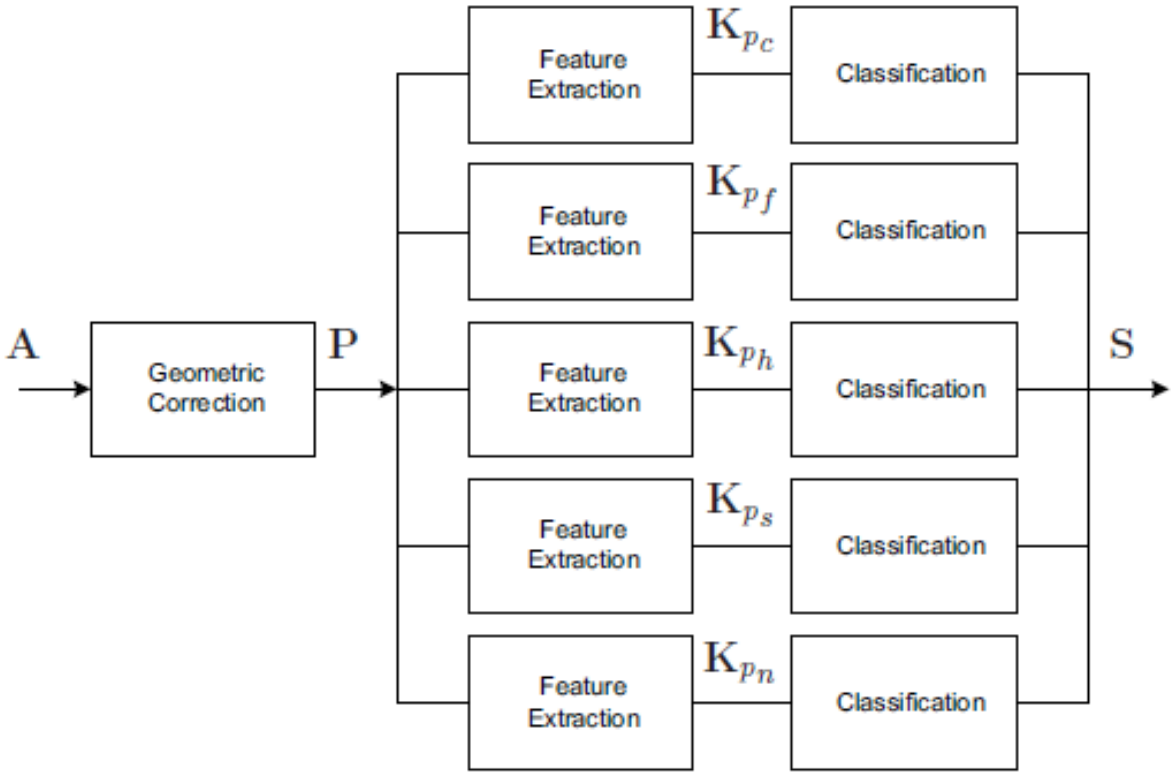

Figure 1 – Block diagram of the scheme for classification of events.

The classification of events in the matrix $\mathbf{A}$ can be formulated as a simple decision between hypotheses related to the occurrence of the events covered in this work, as shown

below:

$$\begin{aligned}
\mathcal{H}_{A,0} &: \mathbf{A} = \mathbf{A}_{crack}, \\
\mathcal{H}_{A,1} &: \mathbf{A} = \mathbf{A}_{flak}, \\
\mathcal{H}_{A,2} &: \mathbf{A} = \mathbf{A}_{head}, \\
\mathcal{H}_{A,3} &: \mathbf{A} = \mathbf{A}_{spall}, \\
\mathcal{H}_{A,4} &: \mathbf{A} = \mathbf{A}_{norm}.
\end{aligned} \tag{2.1}$$

In which $\mathbf{A}_{crack}$, $\mathbf{A}_{flak}$, $\mathbf{A}_{head}$, $\mathbf{A}_{spall}$ and $\mathbf{A}_{norm}$ denotes the cracking, flaking, head check, spalling and normal condition of the rail head, respectively.

2.1 GEOMETRIC CORRECTION

The geometric correction through a two-dimensional affine transformation aims to facilitate the image processing transforming the original image parallel to Y axis of the cartesian coordinate system [15–17]. The affine transformation consists of a linear transformation followed by a translation. This transformation preserves the parallelism property. If two lines are parallel before the transformation, these lines are also parallel after processing. The expression that describes the affine transformation is

$$\begin{bmatrix} x^* \\ y^* \end{bmatrix} = \begin{bmatrix} a & b \\ c & d \end{bmatrix} \cdot \begin{bmatrix} x \\ y \end{bmatrix} + \begin{bmatrix} x_0 \\ y_0 \end{bmatrix}, \tag{2.2}$$

where a, b, c, d, x_0 and y_0 are the parameters of the affine transformation. The variables a, b, c and d comprise a rotation operation and the translation is given by x_0 and y_0. The parameters x and y are the original coordinates and x^* and y^* the transformed coordinates. Figure 2 shows an image before and Figure 3 shows the same image after an affine transformation. Note that the affine transformation also changed the image resolution from 1600×1200 to 1200×1200 pixels.

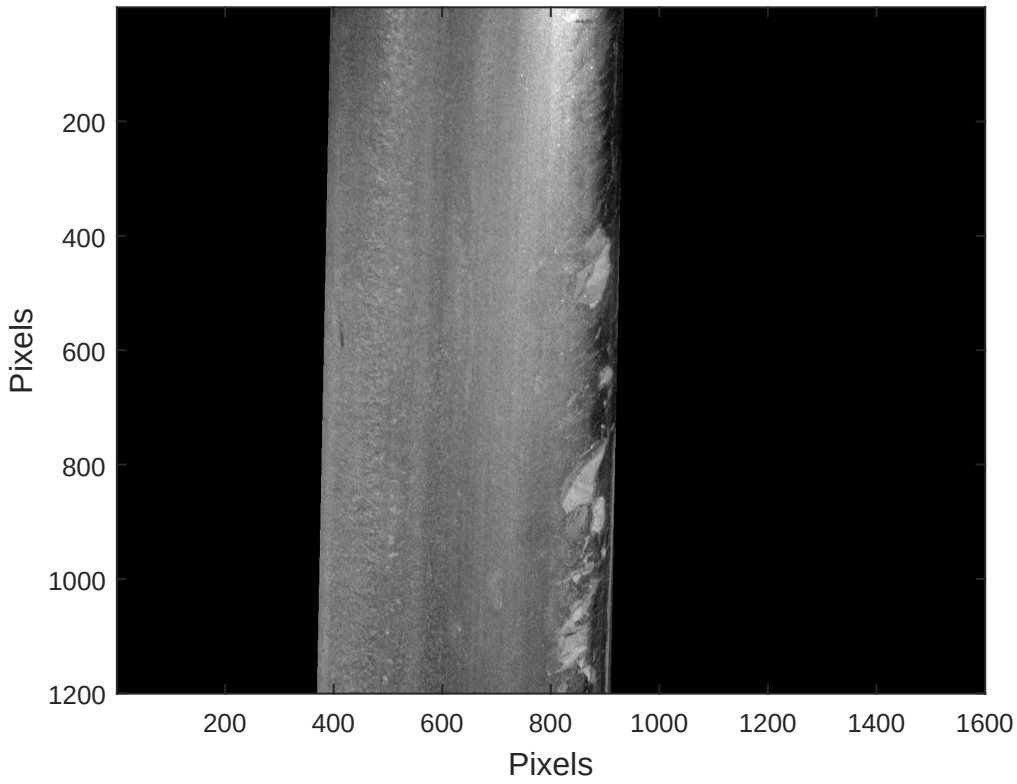

Figure 2 – An example of image when the cracking is considered before the affine transformation.

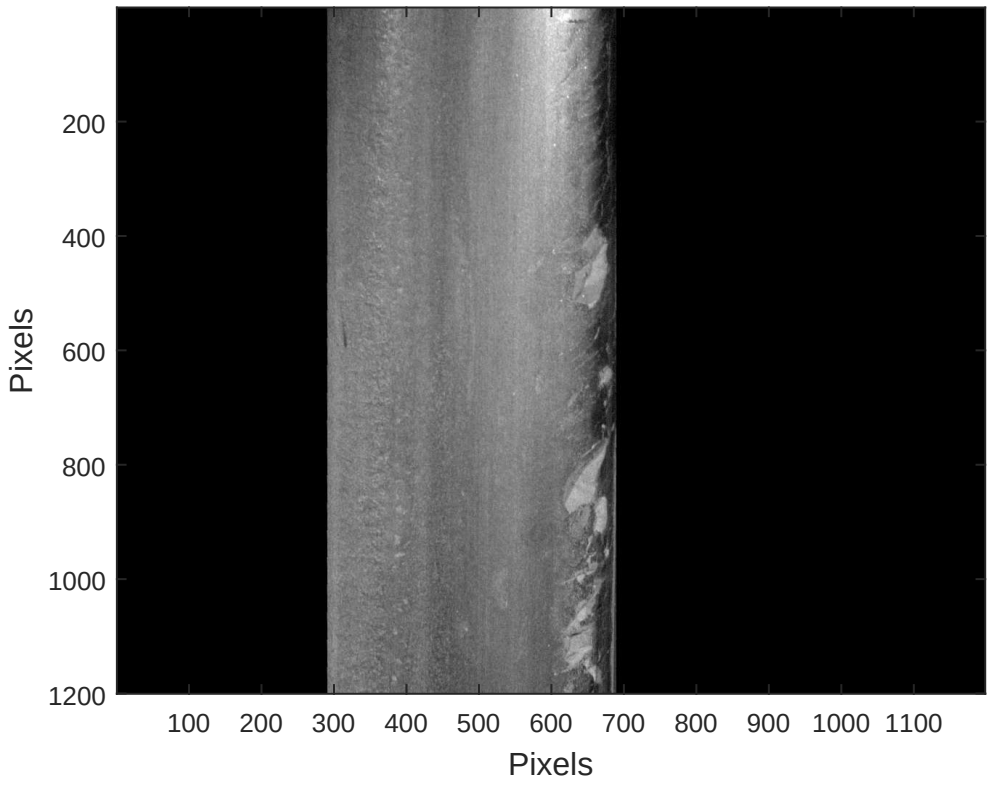

Figure 3 – An example of image when the cracking is considered after the affine transformation.

2.2 FEATURE EXTRACTION BASED ON GRAY LEVEL CO-OCCURRENCE MATRIX

The gray level co-occurrence matrix has been one of the most used methods to analyze textures on images [18–22] and it is a two-dimensional dependence matrix that considers the spatial relationship between neighboring pixels. The GLCM describes the textures of the images based on the frequency in which two gray levels separated by a distance d in a θ direction occur in the image. The texture information of an image can be described by GLCM functions, as shown below

$$G = \begin{bmatrix} p(1,1) & p(1,2) & \cdots & p(1,n) \\ p(2,1) & p(2,2) & \cdots & p(2,n) \\ \vdots & \vdots & \ddots & \vdots \\ p(n,1) & p(n,2) & \cdots & p(n,n) \end{bmatrix}, \tag{2.3}$$

where $p(i,j)$ denotes the value of the matrix element having index (i,j) and n is the number of gray levels present in the image. For the construction of a GLCM, we must define the spatial relationship composed by the distance d, in pixel unit, and the adopted direction from the reference pixel, denoted by θ. Figure 4 shows us the possible angles to be adopted from the reference pixel.

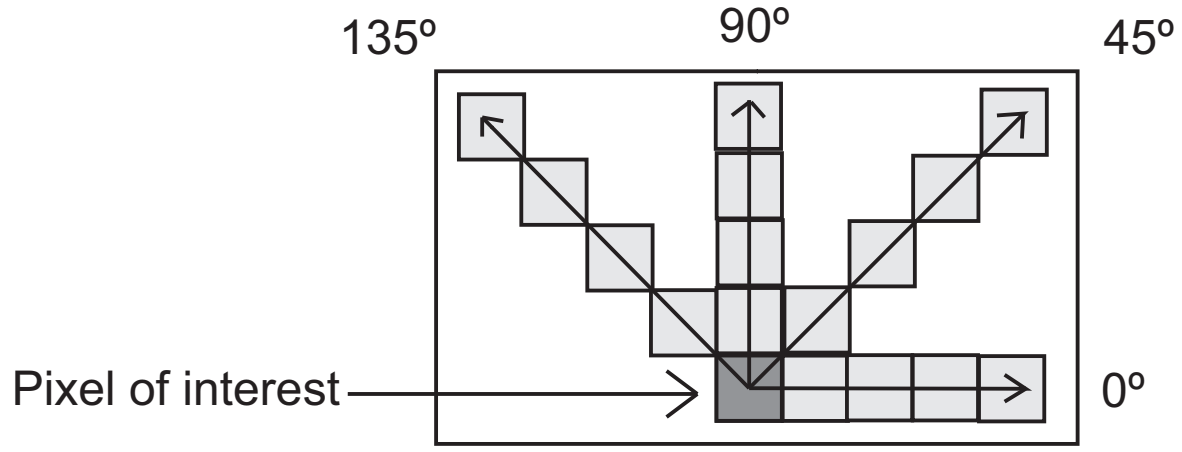

Figure 4 – In addition to $\theta = 0°$, we can choose other three values to the reference angle. Thus, the GLCM provided from Figure 4 has $\theta = \{0°, 45°, 90°, 135°\}$ and $d = 4$.

Figure 5 show us how is calculated an GLCM for $d = 1$ and $\theta = 0°$. The element $p(1, 1)$ contains the value 1 because there is only one instance in the input image where two horizontally adjacent pixels have the values 1 and 1, respectively. The element $p(5, 7)$ contains the value 2 it has two instances where two horizontally adjacent pixels have the values 5 and 7. Thus, each element $p(i, j)$ of the grey level co-occurrence matrix represents the instances there has been a transition from gray level i to j considering the distance d between the two neighboring pixels in the direction θ.

The GLCM can be normalized by dividing each entry by the number of neighboring resolution cell pairs, wich can be expressed by

$$p\left(i,j\right) = \frac{m(i,j)}{\sum_{i=0}^{n}\sum_{j=0}^{n} m\left(i,j\right)}. \tag{2.4}$$

Each value $p(i, j)$ is the probability of a transition between gray levels under specified conditions of distance and direction.

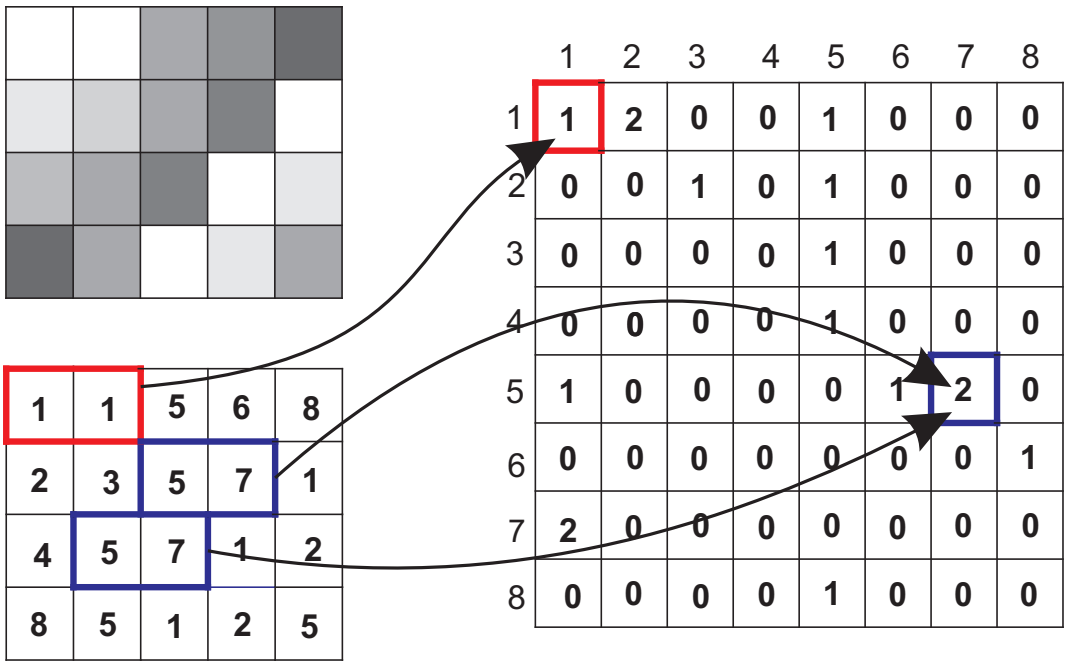

Figure 5 – An example of GLCM construction from a small image, where $d = 1$, $\theta = 0°$ and the gray levels range from 1 to 8.

Based on the normalized co-occurrence matrices [19] [20], we can use the energy, contrast, correlation and homogeneity to represent characteristic textures.

Energy [23, 24], also known as the second angular *momentum*, evaluates the uniformity texture of an image. The expression that describes the energy is

$$ASM(i,j) = \sum_{i=1}^{n}\sum_{j=1}^{n} p(i,j)^2. \tag{2.5}$$

The Contrast [21, 22], also called the variance or inertia, measures the presence of unexpected transitions of gray levels in image. It can be calculated as follows

$$CON(i,j) = \sum_{i=1}^{n}\sum_{j=1}^{n}(i-j)^2 p(i,j). \tag{2.6}$$

Correlation [21, 25], measures the joint probability occurrence of the specified pixel pairs and it returns a measure of how a pixel is correlated with its neighbor along the whole image

$$COR(i,j) = \sum_{i=1}^{n}\sum_{j=1}^{n}\frac{(i-\mu_i)(j-\mu_j)}{\sigma_i\sigma_j}p(i,j), \tag{2.7}$$

where μ_i, μ_j, σ_i and σ_j are the means and standard deviations, respectively.

Homogeneity [25,26], returns a value that measures the proximity of the distribution of elements in GLCM with respect to its diagonal and it is given by

$$HOM(i,j) = \sum_{i=1}^{n}\sum_{j=1}^{n}\frac{p(i,j)}{1+|i-j|}, \tag{2.8}$$

where | | denotes the modulus operator.

It is important to state that all the above mentioned characteristic textures are used as input to the classifiers discussed in this work.

3 PROPOSED MODELS

3.1 TYPE-1 SINGLETON FUZZY LOGIC SYSTEM

Considering singleton fuzzification, max-product composition, product implication and height defuzzifier and leaving open the choice of membership function, it is simple to show that the output of a type-1 and singleton FLS is [27]:

$$f_s(\mathbf{x}) = \frac{\sum_{l=1}^{M} \theta_l \prod_{k=1}^{K_p} \mu_{F_k^l}(x_k)}{\sum_{l=1}^{M} \prod_{k=1}^{K_p} \mu_{F_k^l}(x_k)}, \tag{3.1}$$

where $\mathbf{x} \in \mathbb{R}^{K_p}$ is the vector constituted by the features extracted through the GLCM, $\prod$ denotes the product operator, $m_{F_k^l}$ is the membership function associated to the k-th input feature of the l-th rule, and θ_l is the weight associated with the l-th rule, $l = 1, \ldots, M$. The subscript "s" in $f_s(\mathbf{x})$ makes it clear that this is a type-1 and singleton FLS. Considering the product operator for the t-norm, and assuming that each membership function $\mu_{F_k^l}(x_k)$ is of a Gaussian form, then

$$\mu_{F_k^l}(x_k) = \exp\left\{-\frac{1}{2}\left(\frac{x_k - m_{F_k^l}}{\sigma_{F_k^l}}\right)^2\right\}, \tag{3.2}$$

where $m_{F_k^l}$ and $\sigma^2_{F_k^l}$ are the mean and the variance, respectively.

The type-1 and singleton FLS expressed in equation (3.1) can be represented generically as

$$f_s(\mathbf{x}) = \sum_{l=1}^{M} \theta_l \phi_l(\mathbf{x}), \tag{3.3}$$

where $\phi_l(\mathbf{x})$ is called fuzzy basis function (FBF) [27], that is given by:

$$\begin{aligned} \phi_l(\mathbf{x}) = & \frac{\prod_{k=1}^{p} \mu_{F_k^l}(x_k)}{\sum_{l=1}^{M} \prod_{k=1}^{p} \mu_{F_k^l}(x_k)} \\ = & \frac{\prod_{k=1}^{p} \exp\left(-\frac{\left(x_k^{(q)} - m_{F_k^l}\right)^2}{2\sigma^2_{F_k^l}}\right)}{\sum_{l=1}^{M}\left[\prod_{k=1}^{p} \exp\left(-\frac{\left(x_k^{(q)} - m_{F_k^l}\right)^2}{2\sigma^2_{F_k^l}}\right)\right]}, \end{aligned} \tag{3.4}$$

Given a set of input-output pairs $(\mathbf{x}^{(q)} : y^{(q)})$, where q denotes the qth iteration and each iteration consists of the presentation of all samples, the problem consists, in fact, of minimizing the following cost function [27]:

$$J(\mathbf{w}^{(q)}) = \frac{1}{2}\left[f_s(\mathbf{x}^{(q)}) - y^{(q)}\right]^2. \tag{3.5}$$

The result is

$$m_{F_k^l}(q+1) = m_{F_k^l}(q) - \alpha \left[f_s(\mathbf{x}^{(q)}) - y^{(q)}\right] \times \left[\theta_l(q) - f_s(\mathbf{x}^{(q)})\right] \frac{\left[x_k^{(q)} - m_{F_k^l}(q)\right]}{\sigma^2_{F_k^l}(q)} \phi_l(\mathbf{x}^{(q)}) \quad , \tag{3.6}$$

$$\theta_l(q+1) = \theta_l(q) - \alpha \left[f_s(\mathbf{x}^{(q)}) - y^{(q)}\right] \phi_l(\mathbf{x}^{(q)}) \tag{3.7}$$

and

$$\sigma_{F_k^l}(q+1) = \sigma_{F_k^l}(q) - \alpha \left[f_s(\mathbf{x}^{(q)}) - y^{(q)}\right] \times \left[\theta_l(q) - f_s(\mathbf{x}^{(q)})\right] \frac{\left[x_k^{(q)} - m_{F_k^l}(q)\right]^2}{\sigma^3_{F_k^l}(q)} \phi_l(\mathbf{x}^{(q)}) \quad . \tag{3.8}$$

Note that α is the stepsize used to update parameters from type-1 and singleton FLS.

3.2 TYPE-1 NON-SINGLETON FUZZY LOGIC SYSTEM

Considering non-singleton fuzzification, max-product composition, product implication and height defuzzifier and gaussian membership functions, the output of a type-1 and non-singleton FLS is [27]

$$f_{ns}(\mathbf{x}) = \sum_{l=1}^{M} \theta_l \phi_l(\mathbf{x}), \tag{3.9}$$

where $\phi_l(\mathbf{x})$ is the FBF [27] and is given by

$$\phi_l(\mathbf{x}) = \frac{\prod_{k=1}^{p} \exp\left(-\frac{1}{2}\frac{\left(x_k^{(q)} - m_{F_k^l}\right)^2}{\sigma^2_{F_k^l} + \sigma_X^2}\right)}{\sum_{l=1}^{M}\left[\prod_{k=1}^{p} \exp\left(-\frac{1}{2}\frac{\left(x_k^{(q)} - m_{F_k^l}\right)^2}{\sigma^2_{F_k^l} + \sigma_X^2}\right)\right]}, \tag{3.10}$$

where $\mathbf{x} \in \mathbb{R}^{K_p}$ is the vector constituted by K_p elements, $\prod$ denotes the product operator, $m_{F_k^l}$ and $\sigma_{F_k^l}$ are the mean and variance associated to the k-th input feature of the l-th rule. θ_l is the weight associated with the l-th rule, $l = 1, \ldots, M$. σ_X is the variance associated to each input membership function. The subscript "ns" in $f_{ns}(\mathbf{x})$ informs that this is a non-singleton FLS.

Consider a set of input-output pairs $(\mathbf{x}^{(q)} : y^{(q)})$, where q denotes the qth iteration. To obtain the suitable parameters of $f_{ns}(\mathbf{x})$ for our classification problem, the task is to minimize the following cost function [27]

$$J(\mathbf{w}^{(q)}) = \frac{1}{2}\left[f_{ns}(\mathbf{x}^{(q)}) - y^{(q)}\right]^2. \tag{3.11}$$

By applying Steepest Descent method, we obtain

$$\begin{aligned} m_{F_k^l}(q+1) = m_{F_k^l}(q) - \alpha \left[f_{ns}(\mathbf{x}^{(q)}) - y^{(i)}\right] \times \\ \left[\theta_l(q) - f_{ns}(\mathbf{x}^{(q)})\right] \left[\frac{x_k^{(q)} - m_{F_k^l}(q)}{\sigma_X^2(q) + \sigma_{F_k^l}^2(q)}\right] \phi_l(\mathbf{x}^{(q)}), \end{aligned} \tag{3.12}$$

$$\theta_l(q+1) = \theta_l(q) - \alpha \left[f_{ns}(\mathbf{x}^{(q)}) - y^{(q)}\right] \phi_l(\mathbf{x}^{(q)}), \tag{3.13}$$

$$\begin{aligned} \sigma_{F_k^l}(q+1) = \sigma_{F_k^l}(q) - \alpha \left[f_{ns}(\mathbf{x}^{(q)}) - y^{(q)}\right] \times \\ \left[\theta_l(q) - f_{ns}(\mathbf{x}^{(q)})\right] \sigma_{F_i^l}(q) \left[\frac{x_k^{(q)} - m_{F_k^l}(q)}{\sigma_X^2(q) + \sigma_{F_k^l}^2(i)}\right]^2 \phi_l(\mathbf{x}^{(q)}), \end{aligned} \tag{3.14}$$

and

$$\begin{aligned} \sigma_X(q+1) = \sigma_X(q) - \alpha \left[f_{ns}(\mathbf{x}^{(q)}) - y^{(q)}\right] \times \\ \left[\theta_l(q) - f_{ns}(\mathbf{x}^{(q)})\right] \sigma_X(q) \left[\frac{x_k^{(q)} - m_{F_k^l}(q)}{\sigma_X^2(q) + \sigma_{F_k^l}^2(q)}\right]^2 \phi_l(\mathbf{x}^{(q)}). \end{aligned} \tag{3.15}$$

Note that $\alpha \in \mathbb{R} | 0 \leq \alpha < 1$ is the step size value used to update parameters of the type-1 and non-singleton FLS.

From (3.11), we know that

$$\begin{aligned} \mathbf{w}^{(q)} = \; & \Big[m_{F_1^1}(q), \ldots, m_{F_p^1}(q), \ldots, m_{F_1^M}(q), \ldots, m_{F_p^M}(q), \\ & \sigma_{F_1^1}(q), \ldots, \sigma_{F_p^1}(q), \ldots, \sigma_{F_1^M}(q), \ldots, \sigma_{F_p^M}(q), \\ & \theta_1(q), \ldots, \theta_M(q), \sigma_X(q)\Big] \end{aligned} \tag{3.16}$$

and

$$\begin{aligned} & \nabla J(\mathbf{w}^{(q)}) = \\ & \Big[\nabla_{m_{F_1^1}(q)} J(\mathbf{w}^{(q)}), \ldots, \nabla_{m_{F_P^1}(q)} J(\mathbf{w}^{(q)}), \ldots, \\ & \nabla_{m_{F_1^M}(q)} J(\mathbf{w}^{(q)}), \ldots, \nabla_{m_{F_P^M}(q)} J(\mathbf{w}^{(q)}), \\ & \nabla_{\sigma_{F_1^1}(q)} J(\mathbf{w}^{(q)}), \ldots, \nabla_{\sigma_{F_P^1}(q)} J(\mathbf{w}^{(q)}), \ldots, \\ & \nabla_{\sigma_{F_1^M}(q)} J(\mathbf{w}^{(q)}), \ldots, \nabla_{\sigma_{F_P^M}(q)} J(\mathbf{w}^{(q)}), \\ & \nabla_{\theta_1(q)} J(\mathbf{w}^{(q)}), \ldots, \nabla_{\theta_M(q)} J(\mathbf{w}^{(q)}), \nabla_{\sigma_X(q)} J(\mathbf{w}^{(q)}\Big]^T, \end{aligned} \tag{3.17}$$

denote, respectively, the parameters vector and the gradient vector of a type-1 and non-singleton FLS.

The first-order derivative of $J(\mathbf{w}^{(q)})$ with regard to parameters $m_{F_k^l}(q)$, $\sigma_{F_k^l}(q)$, $\theta_l(q)$ and $\sigma_X(q)$ are

$$\begin{aligned} \nabla_{m_{F_k^l}(q)} J(\mathbf{w}^{(q)}) = \left[f_{ns}(\mathbf{x}^{(q)}) - y^{(q)}\right] \times \\ \left[\theta_l(q) - f_{ns}(\mathbf{x}^{(q)})\right] \phi_l(\mathbf{x}^{(q)}) a_{F_k^l}(q), \end{aligned} \tag{3.18}$$

$$\begin{aligned} \nabla_{\sigma_{F_k^l}(q)} J(\mathbf{w}^{(q)}) = \left[f_{ns}(\mathbf{x}^{(q)}) - y^{(q)}\right] \times \\ \left[\theta_l(q) - f_{ns}(\mathbf{x}^{(q)})\right] \phi_l(\mathbf{x}^{(q)}) b_{F_k^l}(q), \end{aligned} \tag{3.19}$$

$$\nabla_{\theta_l(q)} J(\mathbf{w}^{(q)}) = \left[f_{ns}(\mathbf{x}^{(q)}) - y^{(q)} \right] \phi_l(\mathbf{x}^{(q)}), \tag{3.20}$$

and

$$\begin{aligned} \nabla_{\sigma_X(q)} J(\mathbf{w}^{(q)}) = & \left[f_{ns}(\mathbf{x}^{(q)}) - y^{(q)} \right] \times \\ & \left[\theta_l(q) - f_{ns}(\mathbf{x}^{(q)}) \right] \phi_l(\mathbf{x}^{(q)}) c_{F_k^l}(q). \end{aligned} \tag{3.21}$$

Note that

$$a_{F_k^l}(q) = \frac{x_k^{(q)} - m_{F_k^l}(q)}{\sigma^2_{F_k^l}(q) + \sigma^2_X(q)}, \tag{3.22}$$

$$b_{F_k^l}(q) = \frac{\left(x_k^{(q)} - m_{F_k^l}(q) \right)^2}{\left(\sigma^2_{F_k^l}(q) + \sigma^2_X(q) \right)^2} \sigma_{F_k^l}(q) \tag{3.23}$$

and

$$c_{F_k^l}(q) = \frac{\left(x_k^{(q)} - m_{F_k^l}(q) \right)^2}{\left(\sigma^2_{F_k^l}(q) + \sigma^2_X(q) \right)^2} \sigma_X(q). \tag{3.24}$$

The equations for training type-1 and non-singleton differ from those applied to type-1 and singleton due to the presence of σ_X.

4 EXPERIMENTAL RESULTS

Performance analyses discussed in this section made use of measured data set provided by a company that operates in the railway sector. The data set is composed of images of rail head surface with resolution of 1600×1200 pixels, captured by a camera attached to a special car service that runs through the railway. Three images of the rail head surface are taken per meter.

The acquired images fall within the following five classes: cracking, flaking, head check, spalling and normal condition of the rail head. As a result, there are 88 images for each of the five classes. We show samples of such images in the following five figures 6,7,8,9 and 10.

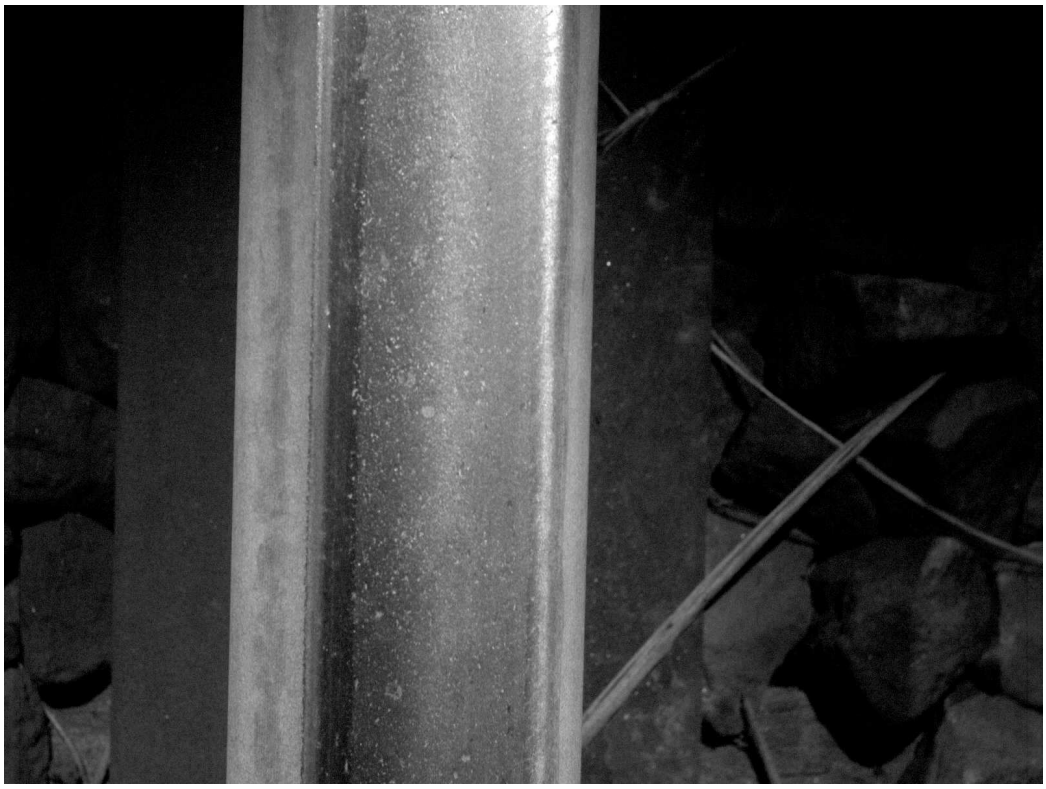

Figure 6 – Typical sample for normal condition class.

Figure 7 – Typical sample for cracking class.

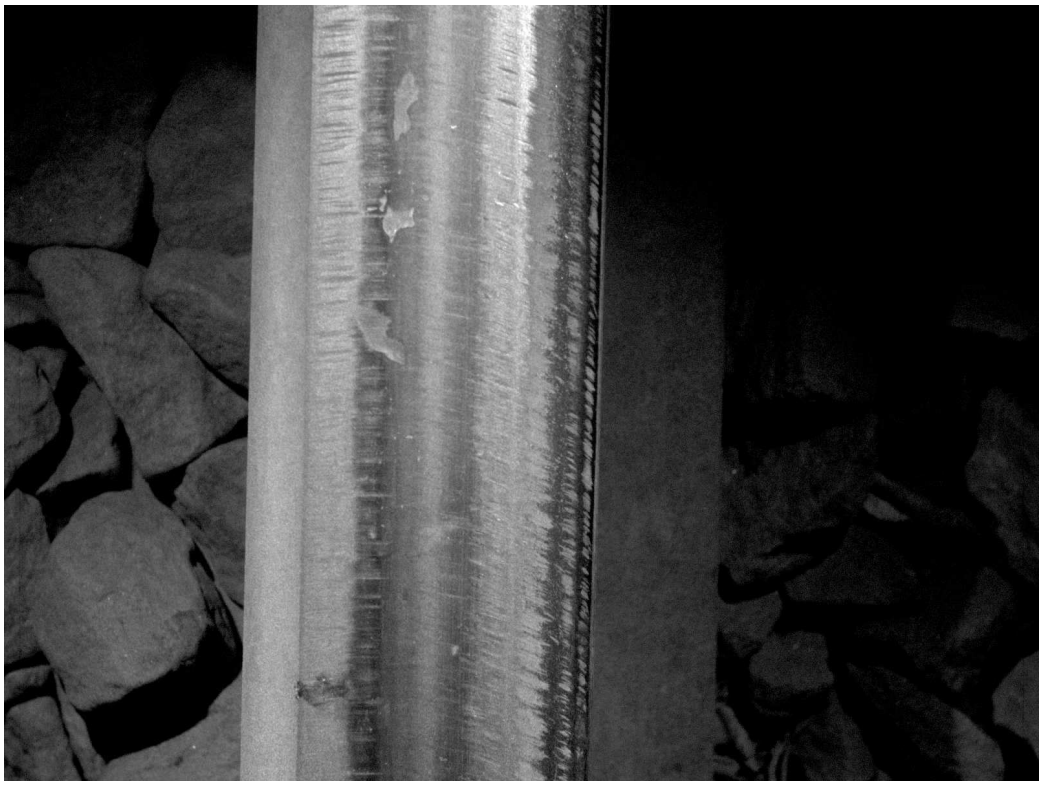

Figure 8 – Typical sample for flaking class.

Figure 9 – Typical sample for head check class.

Figure 10 – Typical sample for spalling class.

Each type-1 and singleton/non-singleton FLS is composed of four rules (M = 4), two rules for the class that has the presence of the event and another two for the class that does not have the presence of the event. The adopted step size for type-1 and singleton/non-singleton FLS trained with the steepest descent method is $\alpha = 0.0001$. The performance gains in term of accuracy and convergence speed are not relevant when $M \neq 4$ or $\alpha \neq 0.0001$. We have initialized the parameters of membership functions heuristically from the calculation of means and variances of the features vector constituted by the elements extracted from the GLCM. Furthermore, we equally and randomly distributed the data set in training and test sets and considered 100 epochs for the training phase.

Following the block diagram of the classification technique depicted in Figure 1, we adopted techniques for geometric correction through affine transformation and feature extraction using GLCM. After evaluating the performance with different features extracted from GLCM, we chose $\theta = \{0°, 45°, 90°, 135°\}$, $d = 100$ and use the obtained features as input of the proposed classifiers. For comparison purpose, we implemented the type-1 and singleton/non-singleton FLS [13, 27] in order to classify defects in a rail head. Observing the block diagram in Figure 1, that $y^{(q)} = 1$ means that the matrix $\mathbf{A}$, constituted by pixels of taken image of the rail head is associated with the occurrence of the defect. On the other hand, $y^{(q)} = -1$ states that the matrix $\mathbf{A}$ is associated with the absence of defect.

4.1 CONVERGENCE SPEED ANALYSIS

Figures 11, 12, 13, 14 and 15, shows the convergence speed for the normal condition, cracking, flaking, head check and spalling classes respectively.

Expressly it can be seen that the singleton model had a higher convergence speed for the classification of normal condition and cracking events. For flaking defect both classifiers had a pretty similar speed convergence, in contrast, for head check and spalling classes the non-singleton FLS had a better performance in this regard.

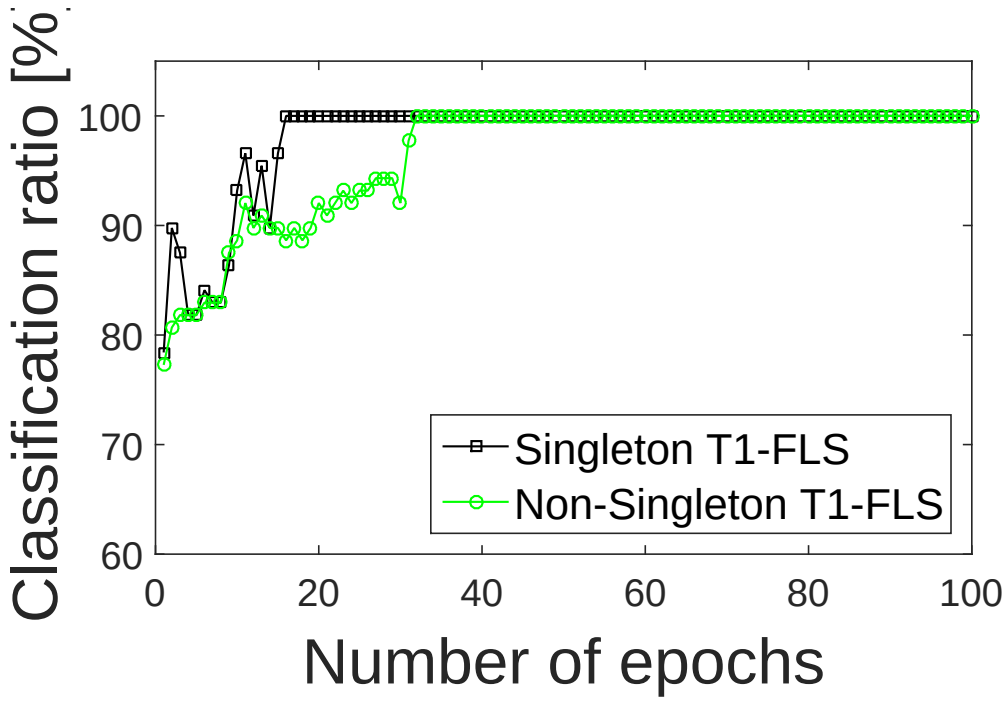

Figure 11 – Convergence speed for normal condition class.

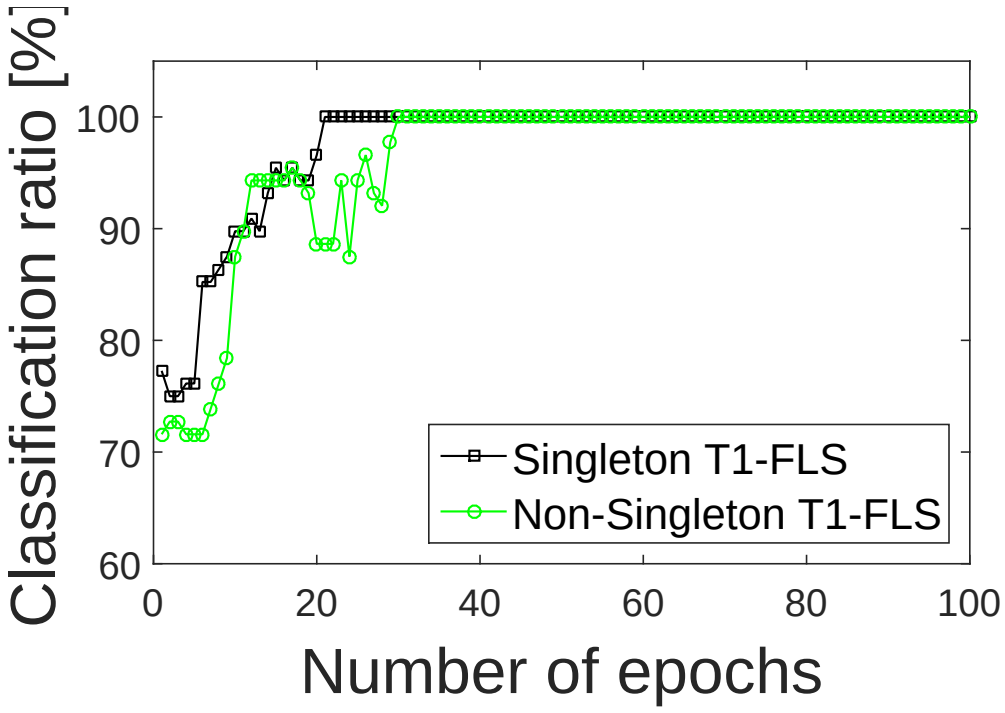

Figure 12 – Convergence speed for cracking class.

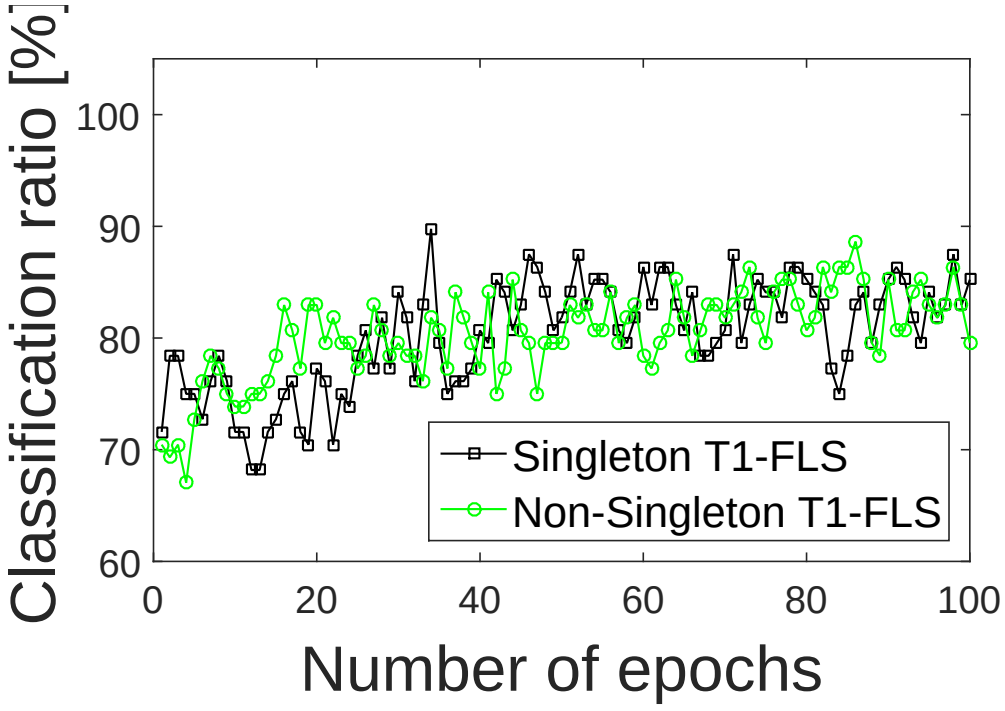

Figure 13 – Convergence speed for flaking class.

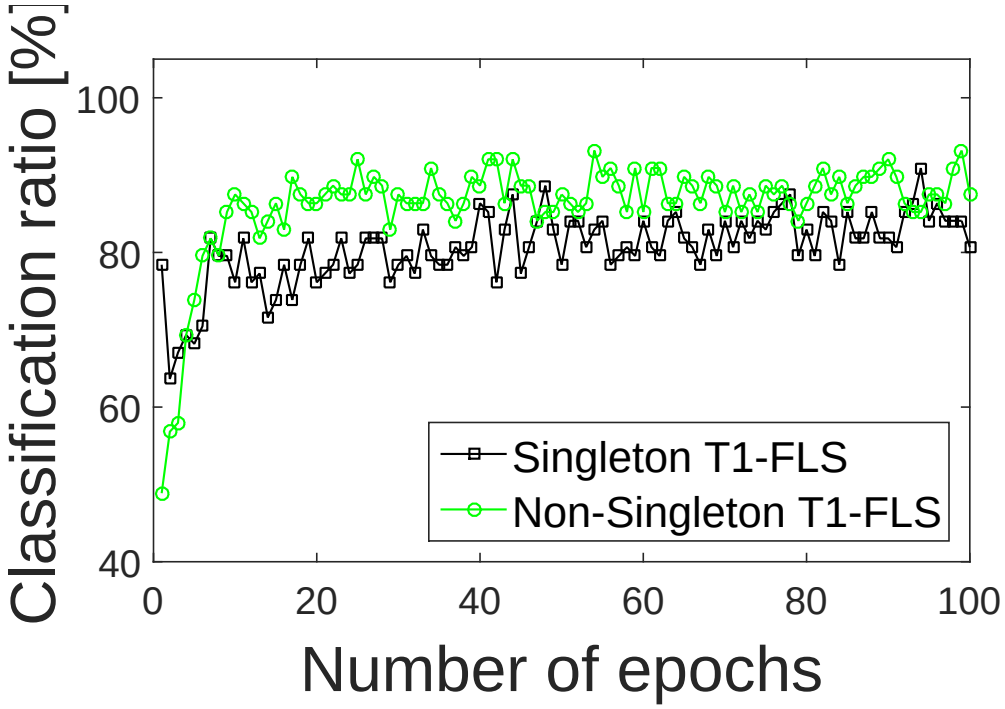

Figure 14 – Convergence speed for head check class.

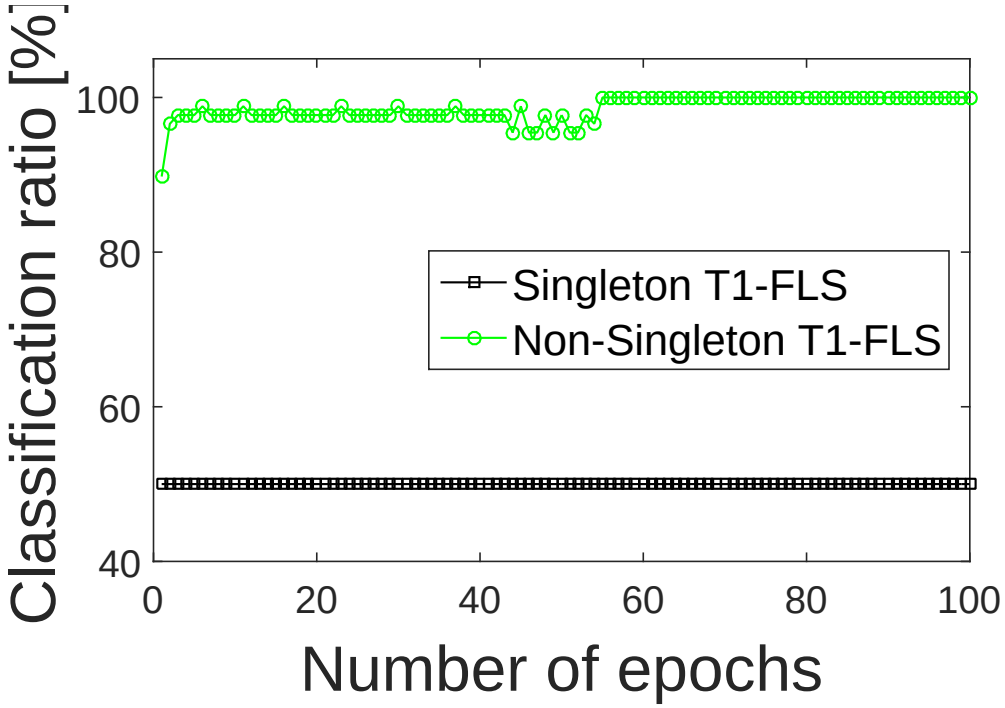

Figure 15 – Convergence speed for spalling class.

Looking for the spalling defect it can be noted a great difference between the two curves, the singleton FLS presented a low performance in relation to the non-singleton FLS for the event classification. This difference was due to a higher degree of uncertainties associated with the measured data regarding to this class. Thus the non-singleton model

assumed a considerably higher performance when data with associated uncertainties were presented to the classifiers.

4.2 CLASSIFICATION RATE ANALYSIS

The numerical results presented in Table 1 indicates the correct classification rates in terms of percentage for the type-1 and singleton/non-singleton FLS, both the training phase and for the test phase. The efficiency ρ is the arithmetic mean of the best achieved performances considering each event. We see that the non-singleton model in addition to having a reasonable speed of convergence, they provide higher efficiency when compared with the type-1 and singleton FLS.

According to the results, the type-1 and singleton FLS had a similar classification rate for the normal condition and cracking events when compared with type-1 and non-singleton FLS, with 100.0% of rate for both. Still analyzing Table 1, we can note that the singleton model has a lower efficiency due to its low rating fee to the spalling event caused by lack of performance when working with data that present uncertainties.

Table 1 – Classification Rate.

Events	Singleton FLS		Non-Singleton FLS	
	Training	Test	Training	Test
Normal Condition	100.0	100.0	100.0	100.0
Cracking	100.0	100.0	100.0	100.0
Flaking	85.2	85.2	79.6	79.6
Head Check	80.7	80.7	87.5	87.5
Spalling	50.0	50.0	100.0	100.0
Efficiency (ρ)	**83.2**	**83.2**	**93.4**	**93.4**

5 CONCLUSIONS

In this work we discussed the use of image processing and computational intelligence techniques, introducing the use of the type-1 and singleton/non-singleton concept aiming to analyze theirs effectiveness to classify typical rail head defects. The geometric correction through a two-dimensional affine transformation and the extraction of GLCM-based features have proved to be relevant and have contributed to consistency and a reduction in the dimensionality of the data to be presented to the classifiers.

Considering a reduced number of epochs, the numerical results obtained through the use of measured data set showed that both models discussed have similar and relevant convergence speed. Additionally, the type-1 non-singleton FLS model reached a higher classification rates than those obtained with the type-1 singleton FLS, specially when there are uncertainties in the input data and the number of epochs in the training phase is limited.

In all analyzed situations the non-singleton model turn out to be an attractive option due to their high classification rate and efficiency reaching percentages in the order of 93.4%. Additionally, it is notorious that non-singleton FLS handled satisfactorily the presence of uncertainties in the measured data showing better classification rates than singleton FLS, thus proving in fact be a attractive choice for the rail head defect classification problem.

Future work is to prototype an equipment to be integrated into the existing rail head supervision system in the company that provided the data of the images. We intend to improve the preprocessing of images, through the research of segmentation tools and other techniques for feature extraction, in order to get a better performance. Also, we plan to investigate the usefulness of non-singleton type-1 FLS to handle the presence of uncertainty in the measured data set.

REFERENCES

[1] Q. Li and S. Ren, "A visual detection system for rail surface defects," *IEEE Transactions on Systems, Man, and Cybernetics*, vol. 42, no. 6, pp. 1531–1542, Nov. 2012.

[2] M. Molodova, Z. Li, A. Nunez, and R. Dollevoet, "Automatic detection of squats in railway infrastructure," *IEEE Transactions on Intelligent Transportation Systems*, vol. 15, no. 5, pp. 1980–1990, Oct. 2014.

[3] G. Karaduman, M. Karakose, and E. Akin, "Experimental fuzzy diagnosis algorithm based on image processing for rail profile measurement," in *Proc. International Symposium Mechatronika*, pp. 1–6, Dec. 2012.

[4] Z. Liu, W. Wang, X. Zhang, and W. Jia, "Inspection of rail surface defects based on image processing," in *Proc. International Asia Conference on Informatics in Control, Automation and Robotics*, vol. 1, pp. 472–475, Mar. 2010.

[5] G. Hu, L. Xiong, and J. Tang, "Heavy rail surface defects detection based on the morphology of multi-scale and dual-structure elements," in *Proc. Chinese Automation Congress*, pp. 2126–2129, Nov. 2015.

[6] L. Jie, L. Siwei, L. Qingyong, Z. Hanqing, and R. Shengwei, "Real-time rail head surface defect detection: A geometrical approach," in *Proc. IEEE International Symposium on Industrial Electronics*, pp. 769–774, Jul. 2009.

[7] H.-Y. Zhang, D. Feng, J. cong Yao, and Y. ling Yu, "Guided wave propagation characteristics in the rail with a crack defect," in *Proc. Symposium on Piezoelectricity, Acoustic Waves and Device Applications*, pp. 1–4, Oct. 2013.

[8] H. Chang, C. Wilson, and J. Jackson, "Eliminating polymer flake defects using an oxygen free chemistry," in *Proc. IEEE International Symposium on Semiconductor Manufacturing Conference Proceedings*, pp. P91–P93, Oct. 1997.

[9] D. Stone, F. Carlson, and C. Bachhuber, "Effect of brake-system components on wheel spalling," in *Proc. IEEE Joint Railroad Conference*, pp. 177–183, Apr. 1999.

[10] V. Vijaykumar and S. Sangamithirai, "Rail defect detection using gabor filters with texture analysis," in *Proc. International Conference on Signal Processing, Communication and Networking*, pp. 1–6, Mar. 2015.

[11] Q. Li and S. Ren, "A real-time visual inspection system for discrete surface defects of rail heads," *IEEE Transactions on Instrumentation and Measurement*, vol. 61, no. 8, pp. 2189−−2199, Aug. 2012.

[12] E. P. de Aguiar, F. M. A. Nogueira, R. P. Amaral, D. F. Fabri, S. C. Rossignoli, J. G. Ferreira, M. M. B. R. Vellasco, R. Tanscheit, P. C. S. Vellasco, and M. V. Ribeiro, "Classification of events in switch machines using bayes, fuzzy logic system and neural network," in *Proc. 15th International Conference on Engineering Applications of Neural Networks*, pp. 81–91, Sep. 2014.

[13] ——, "Eann 2014: a fuzzy logic system trained by conjugate gradient methods for fault classification in a switch machine," *Neural Computing and Applications*, pp. 1–15, 2015.

[14] Q. Liang and J. Mendel, "Interval type-2 fuzzy logic systems: theory and design," *IEEE Transactions on Fuzzy Systems*, vol. 8, no. 5, pp. 535–550, Oct. 2000.

[15] Y. Matsuo, R. Takada, S. Iwasaki, and J. Katto, "Image super-resolution using registration of wavelet multi-scale components with affine transformation," in *Proc. IEEE International Symposium on Multimedia*, pp. 279–282, Dec. 2013.

[16] H. Lin, P. Du, W. Zhao, L. Zhang, and H. Sun, "Image registration based on corner detection and affine transformation," in *Proc. 3rd International Congress on Image and Signal Processing*, pp. 2184–2188, Oct. 2010.

[17] X. Li, Y. Xu, Q. Lv, and Y. Dou, "Affine-transformation parameters regression for face alignment," *IEEE Signal Processing Letters*, vol. 23, no. 1, pp. 55–59, Jan. 2016.

[18] R. Haralick, K. Shanmugam, and I. Dinstein, "Textural features for image classification," *IEEE Transactions on Systems, Man and Cybernetics*, vol. 3, no. 6, pp. 610–621, Nov. 1973.

[19] M. Cui, S. Prasad, M. Mahrooghy, J. Aanstoos, M. Lee, and L. Bruce, "Decision fusion of textural features derived from polarimetric data for levee assessment," *IEEE Journal of Selected Topics in Applied Earth Observations and Remote Sensing*, vol. 5, no. 3, pp. 970–976, Jun. 2012.

[20] V. Thakare and N. Patil, "Classification of texture using gray level co-occurrence matrix and self-organizing map," in *Proc. International Conference on Electronic Systems, Signal Processing and Computing Technologies*, pp. 350–355, Jan. 2014.

[21] H. Nikoo, H. Talebi, and A. Mirzaei, "A supervised method for determining displacement of gray level co-occurrence matrix," in *Proc. 7th Iranian Machine Vision and Image Processing*, pp. 1–5, Nov. 2011.

[22] W. Kun and K. Songtao, "Identification method of waste based on gray level co-occurrence matrix and neural network," in *Proc. International Conference on Materials for Renewable Energy Environment*, pp. 929–931, May. 2011.

[23] J. Yang and J. Guo, "Image texture feature extraction method based on regional average binary gray level difference co-occurrence matrix," in *Proc. International Conference on Virtual Reality and Visualization*, pp. 239–242, Nov. 2011.

[24] Y. Hu, C. xia Zhao, and H. nan Wang, "Directional analysis of texture images using gray level co-occurrence matrix," in *Proc. Pacific-Asia Workshop on Computational Intelligence and Industrial Application*, pp. 277–281, Dec. 2008.

[25] R. Suganya and S. Rajaram, "Feature extraction and classification of ultrasound liver images using haralick texture-primitive features: Application of svm classifier," in *Proc. International Conference on Recent Trends in Information Technology*, pp. 596–602, Jul. 2013.

[26] G. Preethi and V. Sornagopal, "Mri image classification using glcm texture features," in *Proc. International Conference on Green Computing Communication and Electrical Engineering*, pp. 1–6, Mar. 2014.

[27] J. M. Mendel, *Uncertain Rule-Based Fuzzy Logic Systems: Introduction and New Directions*. Prentice Hall PTR, 2001.

APPENDIX A – Publications

The list of papers published during the bachelor's period are as follows:

- E. P. de Aguiar, L. P. V. da Silva, A. F. Moreira, L. G. da Fonseca, F. M. de A. Nogueira, M. M. B. R. Vellasco, and M. V. Ribeiro, "Type-1 Fuzzy Logic System Applied to Classification of Rail Head Defects", *Proc. Brazilian Conference on Fuzzy Systems*, Nov. 2016.
- E. P. de Aguiar, S. V. Machado, L. P. V. da Silva, F. M. de A. Nogueira, L. G. da Fonseca, M. M. B. R. Vellasco, and M. V. Ribeiro, "Set-Membership Type-2 Fuzzy Logic System Applied to Classification of Rail Head Defects", *IEEE Transactions on Intelligent Transportation Systems*, to be submittted.

APPENDIX B – Term of Acceptance

TERMO DE ACEITE PARA REALIZAÇÃO DO TRABALHO DE CONCLUSÃO DE CURSO EM LÍNGUA INGLESA

O presente termo, tem como objetivo acertar entre as partes envolvidas, sendo banca examinadora, orientador, coorientador e discente, a respeito da confirmação da realização em língua inglesa, do Trabalho de Conclusão de Curso, apresentado ao curso de graduação em Engenharia Mecânica, do discente **Lucas Pereira Verneck da Silva**, como requisito parcial para obtenção do título de Bacharel em Engenharia Mecânica.

E, por estarem, assim, de comum acordo, as partes assinam o presente termo para ser anexado à cópia final do Trabalho de Conclusão de Curso.

Juiz de Fora, 10 de Novembro de 2017.

Lucas Pereira Verneck da Silva - Discente
Universidade Federal de Juiz de Fora

Prof. Dr. Eduardo Pestana de Aguiar - Orientador
Universidade Federal de Juiz de Fora

Prof. Me. Renan Piazzaroli Finotti Amaral - Coorientador
Universidade Federal de Juiz de Fora

Prof. Dr. Alexandre da Silva Scari
Universidade Federal de Juiz de Fora

Prof. Dr. Moisés Luiz Lagares Júnior
Universidade Federal de Juiz de Fora

ANNEX A – TERM OF AUTHENTICITY

UNIVERSIDADE FEDERAL DE JUIZ DE FORA
FACULDADE DE ENGENHARIA

Termo de Declaração de Autenticidade de Autoria

Declaro, sob as penas da lei e para os devidos fins, junto à Universidade Federal de Juiz de Fora, que meu Trabalho de Conclusão de Curso do Curso de Graduação em Engenharia de Produção é original, de minha única e exclusiva autoria. E não se trata de cópia integral ou parcial de textos e trabalhos de autoria de outrem, seja em formato de papel, eletrônico, digital, áudio-visual ou qualquer outro meio.
Declaro ainda ter total conhecimento e compreensão do que é considerado plágio, não apenas a cópia integral do trabalho, mas também de parte dele, inclusive de artigos e/ou parágrafos, sem citação do autor ou de sua fonte.
Declaro, por fim, ter total conhecimento e compreensão das punições decorrentes da prática de plágio, através das sanções civis previstas na lei do direito autoral[1] e criminais previstas no Código Penal[2], além das cominações administrativas e acadêmicas que poderão resultar em reprovação no Trabalho de Conclusão de Curso.

Juiz de Fora, _____ de _____ de 20____.

_____	_____
NOME LEGÍVEL DO ALUNO (A)	Matrícula
_____	_____
ASSINATURA	CPF

[1] LEI N° 9.610, DE 19 DE FEVEREIRO DE 1998. Altera, atualiza e consolida a legislação sobre direitos autorais e dá outras providências.
[2] Art. 184. Violar direitos de autor e os que lhe são conexos: Pena – detenção, de 3 (três) meses a 1 (um) ano, ou multa.